

# Wide-field interferometric phase imaging of plasmonic nanoparticles at the subcellular level

Nir A. Turko, Ania Peled, and Natan T. Shaked

*Department of Biomedical Engineering, Faculty of Engineering, Tel Aviv University  
Ramat Aviv 69978, Israel*

## ABSTRACT

We present a new wide-field quantitative photothermal (PT) imaging method of gold nanoparticles (AuNPs), which is suitable for obtaining wide-field holographic molecular specificity in biological samples. To obtain this goal, we built a wide-field interferometric phase microscope and modified it for the excitation of plasmonic resonance in AuNPs, while recording their resultant phase signatures. To check the potential of the AuNPs as interferometric cellular labels, they were conjugated to a glass coverslip and excited with a laser at a wavelength corresponding to their absorption spectral peak. We then acquired an image sequence of the sample phase profile in time without the need for lateral scanning, and analyzed the entire field of view using a Fourier analysis, creating a map of the locations of the AuNPs. We obtained a strong PT signal at AuNPs central locations, exponentially dependent on the distance from their centers. This enabled identification of the central locations of the AuNPs in the chosen field of view. Moreover, these PT signals had shown a linear relation to the illumination intensity, distinguishing them from background noise and out-of-focus particles. To the best of our knowledge, we are the first to record wide-field interferometric PT signals at the subcellular level without the need of total-internal-reflection prisms or scanning.

**Keywords:** Gold nanoparticles, plasmon resonance, interferometric phase microscope, holography, photothermal imaging.

## 1. INTRODUCTION

Super-resolution imaging techniques are at the center of attention for biomedical microscopy in general and molecular imaging in particular. For biological research, applying these methods is essential for better understanding of cellular and sub-cellular micro and nano-structure statics and dynamics. Therefore, developing imaging systems capable of identifying micro and nano-scaled objects is crucial for the progress of research in these fields.

One technique, which have been vastly researched over the past decade and holds great potential for future applications, is the use of gold nanoparticles (AuNPs) as molecular contrast agents in photothermal (PT) imaging<sup>1</sup>. The PT effect can be explained by introducing the concept of surface plasmon resonance (SPR). When applying an electric field on metal using a certain wavelength, SPR in the form of nanostructure oscillations of free electrons is created<sup>2</sup>. AuNPs in particular have large absorption coefficients in relatively narrow spectral bands, depending on their size and shape, where in general, the spectral response of gold nanospheres SPR is within the visible range.

Many optical methods were employed for imaging AuNPs within biological tissues using the PT effect. Some of these methods include differential interference contrast (DIC)<sup>3,4</sup>, optical coherence tomography (OCT)<sup>5,6,7</sup> and heterodyne holography based on total internal reflection (TIR) near-field microscopy<sup>8</sup>. While most systems and methods are indeed capable of imaging AuNPs in various sizes down to the single particle level, they have not been implemented in scan-less mode for creating wide-field quantitative images in-vivo due to point-detection, which necessarily leads to lateral scanning. Alternatively, TIR prism, on which the sample is placed, is required.

In this study, we introduce a novel wide-field interferometric phase microscopy (WF-IPM) system with the capability of quantitatively identifying AuNPs in holographic manner. Due to the wide-field (scan-less) imaging, image acquisition time is reduced while increasing field of view (FOV), and thus increasing overall efficiency of the entire imaging process, relative to the aforementioned optical methods of PT imaging.

## 2. OPTICAL SETUP

The proposed PT-WF-IPM system is presented in Fig. 1. To image the phase signature of photothermally excited AuNPs, we have used a low-coherence off-axis WF-IPM system, based on a Michelson (Linnik's-type) interferometer illuminated by Titanium-Sapphire laser. Additional laser with a wavelength that suits the plasmonic peak resonance of the AuNPs is integrated into the WF-IPM system sample arm to obtain PT imaging.

### 2.1 WF-IPM

Low-noise detection of AuNPs in samples using an off-axis Michelson interferometer was achieved by using the Titanium-Sapphire laser (Micra-5, Coherent) with a tunable center wavelength and spectral bandwidth capabilities as the illumination source. The low-coherence source allowed spectral bandwidth of up to  $\sim 100$  nm and thus a coherence gating of down to  $\sim 3\mu\text{m}$ , maintaining a single interference pattern of the reference arm with the desired sample reflecting layer, while eliminating interferences with back-reflections from various optical elements of the sample arm. This ensured low noise levels originating from the system itself.

The imaging beam leaves the source and goes through a beam expander (L1, L2) – matching the beam spot size to that of the desired FOV upon the sample plane. The beam then reaches a convex-convex lens (L3), which is the first lens of a 4-f configuration with both arms of the subsequent off-axis Michelson interferometer. After lens L3, the beam is split into reference and sample arms by beam splitter BS. On the sample arm, a mirror directs the beam into microscope objective MO (M-40X, Newport), as it focuses on the MO back focal plane and creates the aforementioned 4-f configuration. This configuration creates a plane-wave illumination and is identical for both sample and reference arms. The sample beam is then back-reflected by a microscope slide back into the MO and through the BS and projected onto the CMOS camera (DCC1545M, Thorlabs) by lens L4. The reference beam is back-reflected by a slightly tilted mirror and is projected onto the camera in an off-axis manner with respect to the sample beam, creating an off-axis interference pattern.

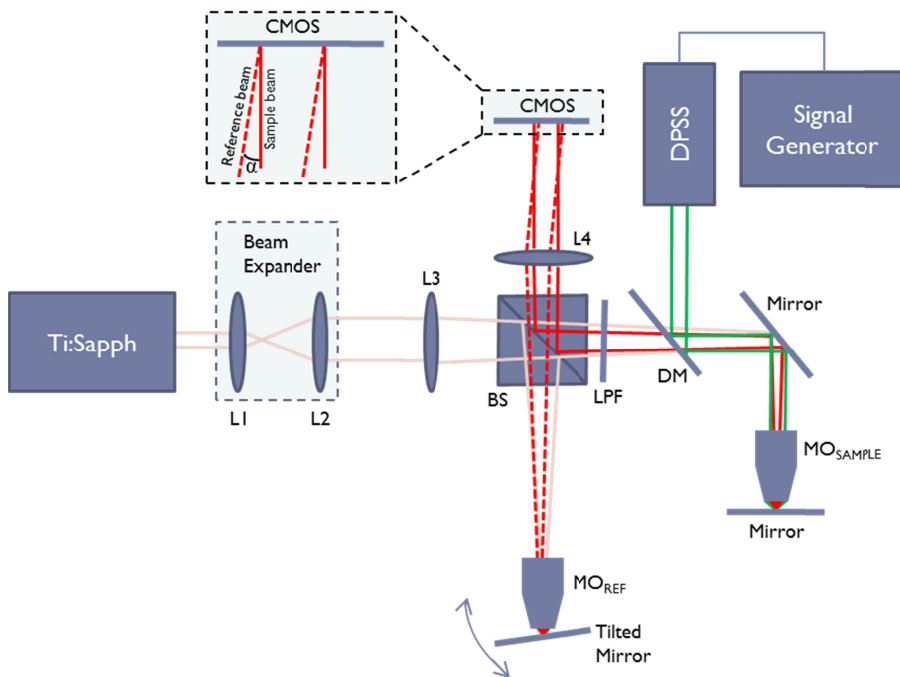


Figure 1. PT-WF-IPM optical setup. Ti:Sapph: Titanium Sapphire laser, DPSS: Diode-pumped solid-state green laser (532nm), L1, L2, L3, L4: Lenses, BS: Beam splitter, LPF: Long pass filter, DM: Dichroic mirror, MO: Microscope objective, CMOS: CMOS digital camera.

## 2.2 PT Excitation

Small diameter (~10nm-90nm) spherical AuNPs usually have peak or near-peak absorption coefficient<sup>2</sup> at the green wavelength of 532nm. This excitation is initiated by diode pump solid state laser DPSS (LRS-0532-PFM-00200-03, Laserglow) connected to a signal generator (DSOX 2002A, Agilent), which modulates the beam at a tunable frequency (we used frequencies in the 20Hz-120Hz range). The green beam is incorporated to the sample arm by dichroic mirror DM (FF593-Di03, Semrock) and passes through the sample MO to focus upon the sample. Long-pass filter LPF (FF01-593/LP, Semrock) prevents green beam back-reflections residue from reaching the camera. For some experiments, we have added a green beam narrower/expander and/or a focusing lens to create a 4-f configuration of the excitation arm with the MO sample, in order to adjust the green spot size – and consequently the power density [W/cm<sup>2</sup>] – upon the sample, to the excitation levels needed.

## 3. DATA PROCESSING

After data acquisition, processing was also comprised of the phase calculation from the off-axis WF-IPM, and then image-sequence time-resolved analysis of the PT signal.

### 3.1 Phase acquisition

The single-axis off-axis interferogram<sup>9</sup> of the sample can be expressed as:

$$I = I_S + I_R + 2\sqrt{I_S I_R} \cos(\varphi(x, y) + kx \sin \alpha), \quad (1)$$

where  $I_S$  and  $I_R$  are the sample and reference intensities, respectively,  $\varphi(x, y) = \Delta n \cdot k \cdot \Delta z$  is the phase term comprised of  $\Delta n$ , the refractive index difference,  $k$  the wavenumber,  $\Delta z$  the thickness of the sample, and  $\alpha$  denotes the reference beam angle relative to the sample beam, upon the camera plane (see Fig. 1). The beam propagation direction dictates  $z$  axis. Axes  $x, y$  are orthogonal to  $z$ . The cosine term of the interference pattern represents spatial phase modulation, the frequency of which depends on the angle  $\alpha$ . For a low-coherence source, however, the interference zone is limited by the coherence length which is equal to  $\lambda^2/[2\sin(\alpha/2) \cdot \Delta\lambda]$ , where  $\lambda$  is the center wavelength and  $\Delta\lambda$  is the spectral bandwidth of the illumination beam. Therefore, our FOV was also limited to represent an area of  $\sim 40 \times 40 \mu\text{m}^2$  upon the sample plane.

The recorded image was then digitally 2-D Fourier-transformed and one of the cross-correlation terms was spatially filtered. After a reverse Fourier-transform, the argument represents the phase of the sample, which can be unwrapped digitally<sup>10</sup>. Note that according to Eq. 1, the phase is a function of the illumination wavelength  $\lambda=2\pi/k$ , local refractive index differences  $\Delta n$  and the physical thickness of the sample  $\Delta z$ .

### 3.2 PT signal acquisition

We used sphere AuNPs with diameters of 55nm and 70nm (A11-55, A11-70, Nanopartz), both strongly absorb 532nm light. This local light absorption produced localized temperature rise and subsequent local variations of the refractive index. As previously demonstrated in Eq.1, the phase signal recorded by the camera explicitly depends on the refractive index. We modulated the excitation beam to illuminate the sample with an excitation frequency of  $\omega_{ex}=30$  Hz, and as can be seen in Fig. 2(a) obtained local phase oscillations on the pixel representing the nanoparticle position. Recording the image sequence at a frame rate higher than twice  $\omega_{ex}$  enabled us to spectrally analyze each pixel of the FOV, and demodulate the spectrum to filter  $\omega_{ex}$  for obtaining the magnitude of local PT-induced oscillations, henceforth the PT signal (Fig. 2(b)). If the beam covers the entire FOV, the PT signal map produces the PT WF-IPM image.

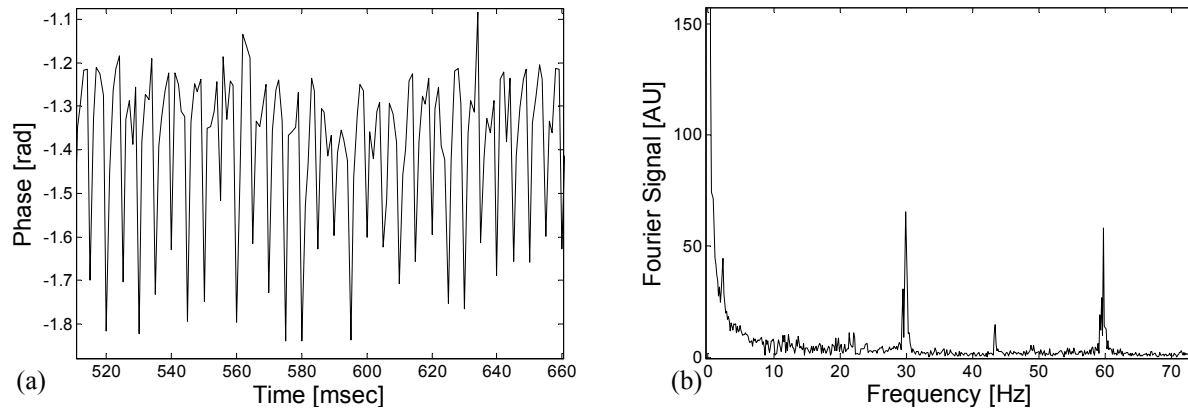


Figure 2. (a) Phase oscillations caused by the PT effect, originated by a 30-Hz excitation of AuNPs at their plasmonic resonance. (b) The corresponding Fourier signal. Except of the modulation frequency (30Hz), second harmonic (60Hz) is also evident.

Analytical analysis for the absorption and heat conductivity was developed elsewhere<sup>3</sup>. We present the spatial profile of the peak to peak phase shift, as<sup>5</sup>:

$$\Delta\varphi_{p-p} = 0.64 \left[ \frac{\partial n}{\partial T} \frac{1}{\kappa} \right] \left[ \frac{I(\vec{r}_0)}{\lambda_0} \right] N\sigma, \quad (2)$$

Where  $\partial n/\partial T$  represents the refractive index variations due to temperature rise,  $\kappa$  the thermal conductivity of the surrounding medium,  $I(\vec{r}_0)$  is the excitation beam intensity at distance  $r_0$  from the AuNP central location,  $\lambda_0$  the imaging central wavelength,  $N$  the number of AuNPs subject to the excitation on the location and  $\sigma$  is the AuNPs absorption coefficient.

For imaging a single AuNP, the system noise levels must be relatively low, according to the calculated phase shift, which is approximately 0.0057 radians for PT excitation with power of  $I \sim 11 \text{ kW/cm}^2$  of our system. Based on this phase shift induced by a single particle, our system should be sensitive enough to image AuNPs accumulations of  $\sim 10$  single nanospheres and above and differentiate them from other particles that do not evoke the PT effect, and thus we obtain molecular specificity in wide-field IPM.

## 4. WIDE FIELD INTERFEROMETRIC IMAGING OF NANOPARTICLES

### 4.1 PT imaging in an aqueous solution

To show the potential for wide-field IPM of nanoparticles in cells, we performed initial PT experiments on an aqueous solution of AuNPs (concentration 2.25 nM). In this case, the mean PT signal is defined as the average signal over a small region of  $\sim 5 \times 5 \mu\text{m}^2$ , overlapped by the excitation beam. Equation 2 determines the PT signal dependency on the excitation beam power, among other factors. By keeping all other parameters constant, the signal should rise linearly with the excitation beam power. Figure 3 demonstrates this linear function. A 250- $\mu\text{m}$  thick chamber, filled with aqueous solution of AuNPs, was imaged and excited at various powers modulated at 114 Hz in time. As described earlier, the PT signal for each pixel was acquired by spectral analysis of the time-resolved change of phase of the sample,  $\Delta\varphi$ . Due to the dynamic profile of the liquid sample, the pixel-by-pixel analysis over the FOV, described earlier, has little meaning and therefore only the spatial average signal was examined. Since the thermal parameters and the concentration (representing  $N$ , the number of AuNPs contributing to the temperature rise) were invariant, the sole contributor to the rise of  $\Delta\varphi$  was  $I_0$ . This suggests that the PT signal was linearly dependent on excitation power, which supports the theoretical analysis.

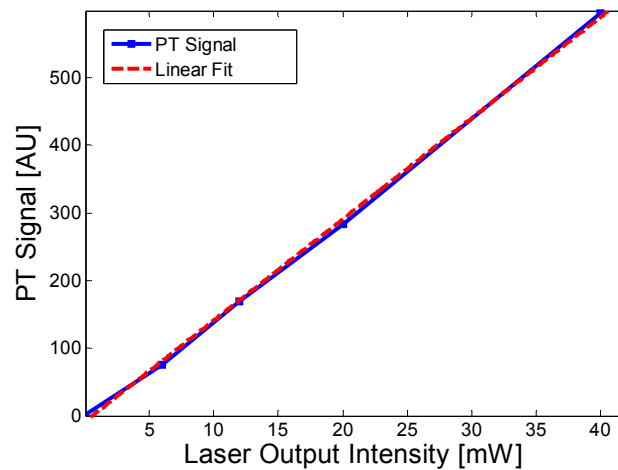


Figure 3. PT signal as a function of the laser power for aqueous solution of AuNPs (70nm, concentration=2.2nM). The signal is the average over a  $\sim 5 \times 5 \mu\text{m}^2$  region.

To test the system capability of identifying AuNPs in a non-dynamic environment, we have prepared samples containing fixed nanospheres and observed the PT signal.

#### 4.2 PT imaging of AuNPs on glass surface

For wide-field interferometric imaging of independent AuNPs, a coverslip covered with AuNPs was placed on the  $40\times$  objective focal plane, as shown in Fig. 1. The sample was imaged onto the CMOS digital camera. In order to create a strong PT signal, the excitation beam diameter was reduced to  $5\mu\text{m}$  and its power varied from 5 to 40mW on the sample plane. These parameters enabled the system to successfully image AuNPs accumulations and aggregates.

Figure 4(a) shows the phase signature of a  $10 \times 10 \mu\text{m}^2$  FOV, containing three AuNP conjugates. This demonstrates the system ability to get a wide-field interferometric PT signal and image several AuNP conjugates simultaneously, without the need for lateral scanning. Possible explanations for non-uniform PT signal strength of the different aggregates are (a) the relatively small beam diameter; (b) the different  $z$  locations of the aggregates; and (c) the different dimensions of the aggregates and the variance of number of nanoparticles creating each of them. AuNP aggregation changes the spectral response of the nanospheres, or  $\sigma$ , as defined in Eq. 2. This degrades our ability to conduct a thorough investigation of the PT signal as a function of aggregate size as it changes the absorption to be more stochastic.

The PT signal as a function of laser power was investigated (Fig. 4(b)) at the peak of the AuNPs aggregate marked by a white arrow. The signal is linearly dependent on laser power, as suggested by Eq. 2.

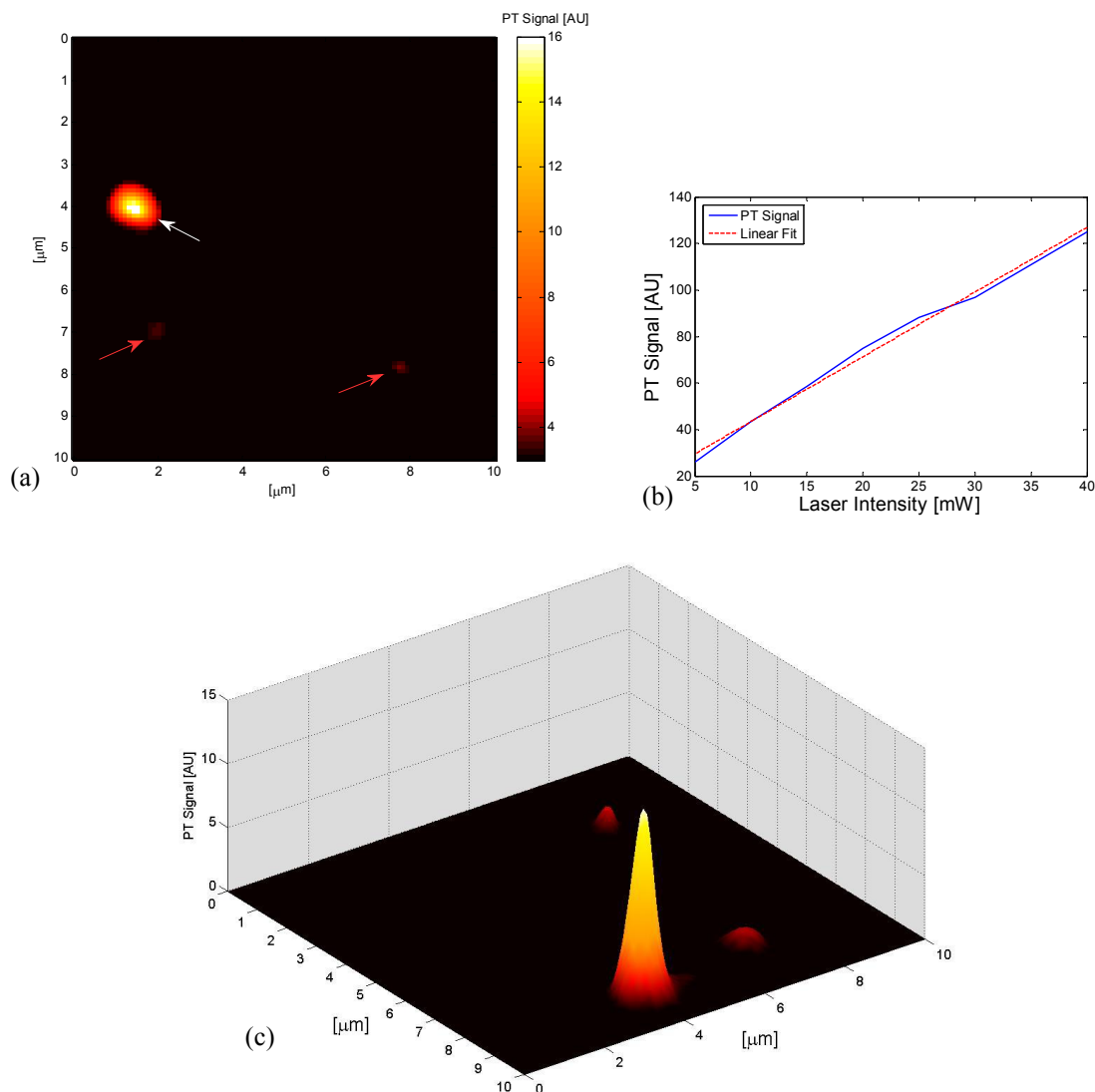


Figure 4. PT signal of non-conjugated AuNPs. (a) PT signals from an area containing AuNPs. The excitation beam diameter was approximately  $5\ \mu\text{m}$ , and it covered the AuNP marked with a white arrow. The two other visible AuNPs were excited by the beam rim and were not visible for low excitation powers. (b) The center pixel power of the signal marked with the white arrow as a function of excitation power. (c) Three-dimensional presentation of the PT signal originating from the AuNPs of the same FOV shown in (a).

## 5. CONCLUSIONS

A novel method for PT wide-field imaging of AuNPs was introduced. The method was based on measuring the change of quantitative phase of the sample as a function of the excitation of the AuNPs. The system was tested to get the signal of AuNP aqueous solution as well as non-conjugated AuNPs aggregates. The linear dependency of both of these signals on the excitation power density was confirmed, matching the theoretical analysis of the system.

With these supporting results, we now extend the use with the system to imaging in cells. The presented system holds great potential in dynamic molecular and cellular imaging. Making lateral scanning obsolete, the time-resolved wide-field signal will be able to track fast cellular processes, as well as add molecular specificity capabilities to WF-IPM by enabling selective imaging of labeled target. As the AuNPs plasmon resonance peak can be tuned by changing their sizes and shapes, different nanoparticles may be bio-conjugated to various functional intra-cellular organelles and image

all of them simultaneously. One practical prospect of our method would be imaging the PT effect of AuNPs in an environment of much thicker objects such as proteins.

## ACKNOWLEDGMENTS

Supported by the German-Israeli Foundation (GIF) grant by the Marie Curie Career Integration Grant (CIG).

## REFERENCES

- [1] Jain P. K., Huang X., El-Sayed I. H., and El-Sayed M. A., "Review of some interesting surface plasmon resonance-enhanced properties of noble metal nanoparticles and their applications to biosystems," *Plasmonics* 2(3), 107-118 (2007).
- [2] Shalaev V. M. and Kawata S., [Nanophotonics with Surface Plasmons], Elsevier, Amsterdam and Oxford, 219-228 (2007)
- [3] Cognet L., Tardin C., Boyer D., Choquet D., Tamarat P., and Lounis B., "Single metallic nanoparticle imaging for protein detection in cells," *PNAS* 100 (20), 11350-11355 (2003).
- [4] Boyer D., Tamarat P., Maali A., Lounis B., and Orrit M., "Photothermal Imaging of nanometer-sized metal particles among scatterers," *Science* 297 (5584), 1160-1163 (2002).
- [5] Skala M. C., Crow M. J., Wax A., and Izatt J. A., "Photothermal optical coherence tomography of epidermal growth factor receptor in live cells using immunotargeted gold nanospheres," *Nano Lett.* 8 (10), 3461-3467 (2008).
- [6] Adler, D. C., Huang, S., Huber R. and Fujimoto J. G., "Photothermal detection of gold nanoparticles using phase-sensitive optical coherence tomography," *Opt. Express* 16(7), 4376-4393 (2008).
- [7] Gaiduk A., Ruijgtok P. V., Yorulmaz M., and Orrit M., "Detection limits in photothermal microscopy," *Chem. Sci.* 1(3), 343-350 (2010).
- [8] Absila E., Tessier G., Gross M., Atlan M., Warnasooriya N., Suck S., Coppey-Moisan M., and Fournier D., "Photothermal heterodyne holography of gold nanoparticles," *Opt. Express* 18(2), 780-786 (2010).
- [9] Mertz J., [Introduction to Optical Microscopy], Roberts & Company, Greenwood Village, Chapter 11 (2010).
- [10] Ghiglia D. C. and Pritt M. D., [Two-Dimensional Phase Unwrapping: Theory, Algorithms, and Software], Wiley, New York (1998).